

Convex Model for Controlled Islanding in Transmission Expansion Planning to Improve Frequency Stability

M. Esmaili, *Senior Member, IEEE*, M. Ghamsari-Yazdel, *Student Member, IEEE*, N. Amjady, *Senior Member, IEEE*, C. Y. Chung, *Fellow, IEEE*

Abstract — Intentional controlled islanding (ICI) is the last resort to split an endangered power system into smaller islands to prevent blackout. New lines that are planned by transmission expansion planning (TEP) can affect the stability of islands during ICI. In this paper, an ICI-TEP method is proposed to improve the stability of islands by more efficient planning of transmission assets. Moreover, by developing a criterion for the frequency of center of inertia (COI) in each island, the frequency deviations of generators from the COI frequency are minimized to result in more stable islands. The proposed ICI-TEP, incorporating AC network representation, is modeled as mixed-integer linear programming and quadratic convex problems ensuring tractability. A Benders decomposition strategy is also proposed to solve the problem. Results of testing the proposed ICI-TEP method on IEEE 39-bus and 300-bus test systems confirm its effectiveness, compared to conventional TEP, in terms of coping with sever disturbances by creating more stable islands with a lower load shedding.

Index terms — Transmission expansion planning, intentional controlled islanding, convex optimization, center of inertia, frequency stability.

NOMENCLATURE

Indices/sets

$k \in \mathcal{K}$	Index and set for islands (subgraphs).
$\ell \in \mathcal{E}_k$	Index and set for all lines in island k .
$l \in \mathcal{L}_k$	Index and set for candidate lines in island k .
$i, j \in \mathcal{V}_k$	Indices and set for buses in island k .
$g \in \mathcal{G}_k$	Index and set for generators in island k .
$t \in \mathcal{T}$	Index and set for planning periods.

Parameters

IC_l	Investment cost of candidate line l .
S_b	System base MVA.
$\tau_{k,t}$	Operation duration of island k at period t .
π_t	Value of lost load at period t .
σ	Discount rate of investment.
$a_{k,g,i,t}$	Binary parameter that is 1 if generator g is at bus i in island k at period t ; 0 otherwise.
$b_{k,\ell,i,j}$	Binary parameter that is 1 if line ℓ is from bus i to bus j in island k ; 0 otherwise.
$c_{k,\ell,i}$	Binary parameter that is 1 if line ℓ is connected to bus i in island k ; 0 otherwise.
$P_{i,t}^D, Q_{i,t}^D$	Active & reactive loads at bus i in period t .

G_i^s, B_i^s	Shunt conductance and susceptance of bus i .
S_ℓ^U	Upper limit for apparent power of line ℓ .
G_ℓ, B_ℓ	Conductance and susceptance of line ℓ .
V_i^L, V_i^U	Lower and upper limits for voltage of bus i .
C_g^{OP}	Operation cost of generator g .
P_g^{GL}, P_g^{GU}	Lower and upper limits for active power of generator g .
Q_g^{GL}, Q_g^{GU}	Lower and upper limits for reactive power of generator g .
$\theta_{i,j}^L, \theta_{i,j}^U$	Lower and upper limits for angle difference across line ij .
M	A positive big value.

Variables

$P_{k,g,t}^G, Q_{k,g,t}^G$	Active and reactive powers of generator g in island k and period t .
$\Delta\omega_{k,g,t}$	Speed deviation of generator g from COI frequency in island k and period t .
$\psi_{k,i,t}$	Proportion of load shedding to load demand at bus i in island k and period.
$f_{k,\ell,t}, g_{k,\ell,t}$	Auxiliary variables for active and reactive line flows.
$P_{k,\ell,t}, Q_{k,\ell,t}$	Active and reactive flows of line ℓ in island k and period t .
$x_{l,t}$	Binary planning variable that is 1 if line l is planned at period t ; 0 otherwise.
$\alpha_{k,i,t}, \beta_{k,i,j,t}$	Transformed variables for convexification.
$\gamma_{k,i,j,t}$	Transformed variable for convexification.
Other symbols are defined in the text as required.	

I. INTRODUCTION

A. Motivation and Background

Recent trends in power systems, such as increasing penetration level of renewable energy sources and increasing use of transmission capacity in electricity markets, have reduced the stability margins and therefore made these systems more vulnerable to severe disturbances [1]. As major disturbances may initiate high impact events, especially in stressed networks, partial or total blackouts may occur with grave economic and social consequences. For instance, the US-Canadian blackout in 2003 affected about 50 million people, and two major blackouts occurred in Sweden and Italy in the same year [1]. Another blackout in 2007 affected about 480,000 customers in Australia [2]. A recent partial blackout in 2019 left 73,000 customers without electricity in New York as a result of a transformer failure [3].

Although power systems are designed to withstand credible

M. Esmaili (corresponding author) and C. Y. Chung are with the Department of Electrical and Computer Engineering, University of Saskatchewan, Saskatoon, SK S7N 5A9 Canada (E-mail: m.esmaili@usask.ca, msdesmaili@gmail.com; c.y.chung@usask.ca).

M. Ghamsari-Yazdel and N. Amjady are with the Department of Electrical and Computer Engineering, Semnan University, Semnan, Iran (E-mail: ghamsari@birjand.ac.ir, amjady@semnan.ac.ir).

contingencies, they may experience challenging operation in fault situations, especially those including the failure of primary protections. In case of failure in the primary protection, faults may be cleared by the backup protection, which operates after an intentional delay [4]. This intentional delay is considered to provide sufficient time for local relays to possibly clear the fault. However, the persistence of faults becomes longer due to the intentional delay of backup protections. As a result, fault durations with orders of a few hundreds of milliseconds are practically possible [1], [5].

Intentional controlled islanding (ICI) is the last resort as a corrective control action to prevent partial or global blackout in large-scale power systems [1]. Following major disturbances, if available control actions are unable to keep a power system intact, ICI can mitigate the disaster by creating stable and sustainable islands [6]. The islands are created considering different features including coherent groups of generators, generation adequacy in islands, and minimum power flow disruption on healthy branches. Depending on the disturbance location and severity, different ICI scenarios are usually planned *a priori* to be implemented in real-time actions [7], [8], [9]. After islanding, system restoration should be done to reintegrate the islands considering their synchronization and stability issues.

Transmission expansion planning (TEP) is carried out to identify optimal network requirements to supply prospective demands in a secure and economic manner. Because planned lines affect power system stability, some preventive/corrective actions may be incorporated into TEP as long-term solutions to reinforce the system against blackouts. Weak transmission corridors are usually selected to be opened in ICI to minimize power flow disruptions in islands [9]. Thus, an ICI-oriented TEP (ICI-TEP) framework can improve system performance by enhancing the stability of islands in ICI events through more efficient planning of candidate lines. Out of different stability types, frequency stability is of concern for any disturbance causing a large loss of load or generation [10]. The frequency of center of inertia (COI) criterion has recently captured attention in power system stability studies [11], [12], [13]. The COI frequency is defined as the common synchronous frequency, to which generators tend in their steady-state conditions [12]. Managing the COI frequency reduces the drift of generator angles [12].

Studying the ICI with a DC network model may lead to infeasible islands mainly due to out-of-bound voltages and local shortage/surplus of reactive power [9], [14]. However, inclusion of nonlinear AC power flow equations can turn the AC-based ICI-TEP model into a mixed-integer nonlinear programming (MINLP) problem, which is computationally demanding and probably intractable in large-scale systems. To this end, linearized or convex formulations of AC network model are proposed in the literature [9], [15], [16]. The convex models can be efficiently solved using available solvers to achieve globally optimal solutions in a reasonable time [15].

B. Literature Review

ICI is addressed in the literature using DC and AC network models. In [9], ICI is formulated with AC network models to minimize power flow disruption and load shedding with grouping of coherent generators. Power flow equations are linearized

around the base point (unity for bus voltage magnitudes and zero for line angle differences) using a piecewise linearization. However, since the base point may differ for each bus in real applications, linearization accuracy may be affected. Also, the piece-wise linearization introduces new integer variables, which may make the model intractable when other modules, such as TEP, are imposed. In [1] and [7], an ICI algorithm with a DC network model is proposed by relaxing a mixed-integer linear programming (MILP) model into a linear programming (LP) problem solved by a recursive procedure.

TEP with different features has also been reported in the literature. A dynamic TEP (including time-dependent investment decisions) with an AC network model can be computationally demanding. Thus, it is usually limited to small test cases in the literature. A dynamic TEP is proposed in [17]; however, a DC network model is used. A bi-level single-period TEP with AC optimal power flow (AC-OPF) constraints is proposed in [18] using the second order cone (SOC), McCormick, and big- M relaxations. Authors in [19] considered short-circuit levels in dynamic TEP and linearized power flow and impedance equations to achieve an MILP model. However, to the best of the authors' knowledge, the effects of transmission planning on ICI scenarios have not been addressed in the literature.

The COI frequency concept has been studied in a number of works. In [11], a method is proposed to estimate COI frequency in online applications by decomposing swing equations of generators. An expression is obtained in [12] to determine COI frequency through a linear combination of bus frequencies. In [13], the center of gravity concept is proposed to estimate local frequencies from the COI frequency.

C. Contributions and Organization of the Paper

In light of the literature review, the main contributions of this paper can be summarized as follows:

- Incorporating ICI scenarios into TEP. This can increase the resiliency of transmission systems against major disasters and extreme contingencies through more efficient planning of transmission assets. Consequently, blackout risk is reduced.
- Enhancing frequency stability of islands in the proposed ICI-TEP. After deriving the frequency of COI for each island, the frequency deviations of generators from the COI frequency are minimized in every island. As a result, the stability of islands improves. Moreover, the proposed ICI-TEP model incorporates AC network representation, which makes it possible to create more voltage secure islands by modeling voltage- and reactive power-related issues.
- Presenting a Benders decomposition (BD) strategy to solve the proposed ICI-TEP problem. This strategy decomposes the ICI-TEP problem into a small-scale integer linear programming (ILP) problem and three quadratic convex (QC) problems to improve tractability and solution optimality.

It is worth noting that the current paper presents a deterministic version of the proposed model for clarity and for better presenting the underlying ideas. However, it can be extended to incorporate power system uncertainties using available uncertainty modeling approaches, such as stochastic programming

approaches that model uncertainties using scenarios [20], robust optimization approaches that model uncertainties using bounded intervals [17], and information-gap decision theory (IGDT) methods that model uncertainties using uncertainty horizons [21]. All of these approaches require a deterministic model of the problem and start from it to characterize the uncertainties. Thus, to extend the proposed deterministic ICI-TEP model to consider the associated uncertainties, which can be taken into account in the future works, having an efficient ICI-TEP model improving frequency stability provides an effective starting point.

The rest of this article is organized as follows. In Section II, the frequency deviation of generators after islanding is modeled using the COI frequency concept. The proposed ICI-TEP framework is formulated in Section III using a BD strategy; the solution procedure is also detailed in this section. Case studies and numerical results are presented in Section IV. Finally, Section V concludes the paper.

II. MODELING THE STABILITY OF ISLANDS USING THE COI FREQUENCY CONCEPT

An integrated power system before islanding can be considered in a steady-state operating point at its steady frequency, which also represents the generators' speed. Following a severe disturbance (which may lead to islanding), unbalance occurs between power generation and consumption, a matter that perturbs frequency by accelerating or decelerating generators. Swing equations of a generator describing its transient behavior are expressed as [11]:

$$\frac{d\delta}{dt} = \omega - \omega_0, \quad (1a)$$

$$\frac{2H}{\omega_0} \frac{d\omega}{dt} = P_m - P_e - K_D(\omega - \omega_0), \quad (1b)$$

where δ and ω are the rotor angle and speed of the generator, respectively after the disturbance; ω_0 is the steady-state synchronous speed before the disturbance; H is the generator inertia constant; P_m is the generator mechanical input power; P_e is the generator output power after the disturbance; and K_D is the generator damping coefficient. Note that this damping parameter is different from the frequency-sensitive load change used in some works, such as [22], to model the power consumption dependency of loads on frequency. Because turbine governors usually have long time constants compared to electrical parameters, P_m can be assumed fixed in transient stability analysis [11]. In addition, some higher-order parameters, such as those associated with transformer tap changers, can also be assumed constant during the short study period of islanding. Integrating (1b) results in:

$$\int_{\omega=\omega_0}^{\omega} \frac{2H}{\omega_0} d\omega = \int_{t=0}^t \{P_m - P_e - K_D(\omega - \omega_0)\} dt, \quad (2)$$

where $t = 0$ corresponds to the instant that the disturbance occurs. Considering a short time period Δt after disturbance and evaluating electrical power $P_{e,t}$ and speed ω_t as two constants at $t = \Delta t$, (2) can be approximated as:

$$\frac{2H}{\omega_0} (\omega_t - \omega_0) \approx \{P_m - P_{e,t} - K_D(\omega_t - \omega_0)\} \Delta t, \quad (3)$$

where $\Delta\omega = \omega_t - \omega_0$ is the generator speed deviation after the disturbance; $\Delta P = P_{e,t} - P_m$ is the change in the generator active output power after the disturbance.

Depending on the time varying variables P_e and ω at the right-hand side of (2), the approximation accuracy of (3) can be evaluated at two scenarios: (i) P_e is low compared with P_m during the fault due to low voltage magnitude at generator terminals. The term $K_D(\omega - \omega_0)$ is also small since generator speed ω is close to the pre-disturbance speed ω_0 in the transient stability study period, and K_D is small [23]. Then, since P_m is dominating in (2), the term under integration is almost constant and can be taken out of the integration leading to (3); (ii) P_e is not low compared with P_m . Although, the term under integration in (2) is time varying, the approximation still holds enough accuracy. Note that we are not trying to estimate the nonlinear function in (2); instead, we estimate the integral value. Further analysis in this regard is presented in Section IV.

By rearranging (3), we obtain a linear approximation for the generator speed change, i.e. $(2H/\omega_0)\Delta\omega \approx -(\Delta P + K_D\Delta\omega)\Delta t$, which can be solved for $\Delta\omega$ as:

$$\Delta\omega \approx \frac{-\Delta t}{2H/\omega_0 + K_D\Delta t} \Delta P = \mu\Delta P, \quad (4)$$

where $\mu = -\Delta t/(2H/\omega_0 + K_D\Delta t)$ is a constant for a given generator. Consequently, the speed of generator g at time Δt after the disturbance is given as:

$$\omega_g \approx \omega_0 + \Delta\omega_g = \omega_0 + \mu_g\Delta P_g. \quad (5)$$

Eq. (5) expresses the speed of generator g (ω_g) as a function of its power disruption (ΔP_g) that occurs due to the disturbance. In this equation, ω_0 and μ_g are constants.

Considering the fact that the splitting of a power system into islands is decided by grouping of coherent generators [6], each island experiences a new frequency of COI after islanding. The frequency of COI is the frequency, to which generator speeds converge in steady state. The frequency of COI for each island is given as [11], [12], [13]:

$$\omega_{COI} = \frac{\sum_{\forall g} H_g \omega_g}{\sum_{\forall g} H_g}, \quad (6)$$

where ω_{COI} is the COI frequency of the island determined by all generators of the island; and H_g is the inertia constant of generator g in the island. By substituting (5) in (6) and with some mathematical manipulations, (6) can be rewritten as:

$$\omega_{COI} = \omega_0 + \frac{\sum_{\forall g} (\mu_g H_g \Delta P_g)}{\sum_{\forall g} H_g}. \quad (7)$$

Eq. (7) gives the frequency of COI for each island as a function of the pre-islanding frequency (ω_0) and power disruptions (ΔP_g) that generators incur after islanding.

To maximize the stability of islands after ICI and to reduce the amount of load shedding that is required to maintain the stability of the islands, the speed deviations of generators from the

island's COI frequency should be minimized in each island. In other words, because ω_{COI} is the target speed for island's generators in the steady-state condition, minimizing the deviation will ease the convergence trajectory of generator speeds toward ω_{COI} .

The speed deviation of each individual generator from the island's ω_{COI} is given as $\Delta\omega_g = \omega_g - \omega_{COI}$. By substituting ω_g and ω_{COI} from (5) and (7), respectively, and after mathematical manipulations, we obtain:

$$\Delta\omega_g = \frac{\mu_g \Delta P_g \sum_{\forall g} H_g - \sum_{\forall g} (\mu_g H_g \Delta P_g)}{\sum_{\forall g} H_g}. \quad (8)$$

Eq. (8) expresses the speed deviation of generator g from the island's COI frequency ($\Delta\omega_g$) as a function of power disruptions applied to generators ($\Delta P_g, \forall g$) due to islanding. Note that $\Delta\omega_g$ can be positive or negative for a specific generator depending on its comparative speed with respect to other generators in the island. In the next section, we use (8) to minimize the total deviations of generator speeds from the COI frequency to improve the frequency stability of islands after ICI.

III. PROPOSED MODEL AND SOLUTION SCHEME FOR ICI-TEP

The overall solution procedure proposed to solve the ICI-TEP problem is illustrated in Fig. 1 using a BD strategy including a master problem (MP) and three subproblems (SPs). This approach enhances the transparency of the ICI-TEP solution in terms of decomposing different objectives of the problem. The MP optimizes the investment decisions, SP1 eliminates infeasibilities considering operational and technical constraints, SP2 minimizes operation costs and power disruptions of islands, and SP3 minimizes frequency deviations of generators from the island's COI frequency as another objective function. The steps of Fig. 1 are detailed in the ensuing subsections. Note that coherent generators usually do not change as a result of adding new lines in TEP based on the slow coherency criterion [24].

A. Graph-Based Representation of Islanding Scenarios

A power system can typically be represented by a graph $\mathcal{G} = (\mathcal{V}, \mathcal{E})$ where \mathcal{V} is the set of nodes (buses) and \mathcal{E} is the set of edges (lines). Each credible severe fault results in its corresponding ICI scenarios. It is expected that the outcome of the proposed method changes if a different set of faults are employed. Set \mathcal{K} includes all probable islands (i.e., subgraphs) that may be created in ICI scenarios in a TEP planning horizon. The island $k \in \mathcal{K}$ is a subset of the main graph ($\mathcal{G}_k \subset \mathcal{G}$) and is represented by its own set of generators \mathfrak{G}_k , buses \mathcal{V}_k , and lines \mathcal{E}_k . We assume the integrated system as the first element of \mathcal{K} ($k = 1$) denoting the normal pre-islanding state. All ICI subgraphs start from $k = 2$. We also assume that subgraphs \mathcal{G}_k ($\forall k \geq 2$) are determined *a priori* using appropriate ICI approaches, such as those presented in [1], [7], considering coherent generators and cut-sets. Note that since the proposed ICI-TEP method foresees ICI scenarios, in order to minimize the investment cost, it does not typically plan new lines in cut-sets, which would be opened in ICI scenarios.

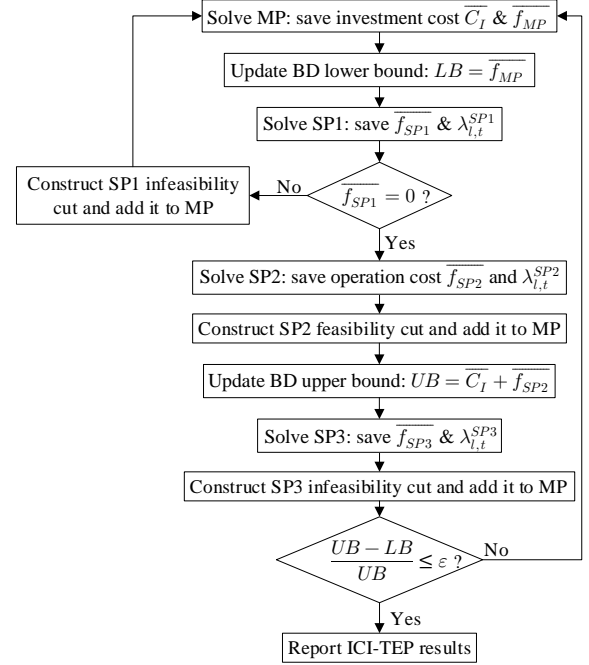


Fig. 1. Proposed solution method for the ICI-TEP problem.

B. Master Problem (MP): Obtaining Optimal Investment Plan

The total cost of the ICI-TEP problem includes the investment cost, operation cost, and islands' load shedding (LS) cost. These cost terms are decomposed between the MP and SPs. The MP minimizes the net present value (NPV) of the time-dependent investment cost in (9) as a small ILP problem. Since $\mathcal{G}_k \subset \mathcal{G}_1$ ($\forall k \geq 2$), $l \in \mathcal{L}_1$ in (9a) includes candidate lines of \mathcal{G}_1 that contain all candidate lines. If a decision is made to build a line at time period t , (9b) makes it available at subsequent periods.

$$\text{Min } f_{MP} \geq \sum_{\forall l \in \mathcal{L}_{1,t}} \frac{IC_l(x_{l,t} - x_{l,t-1})}{(1 + \sigma)^{t-1}}. \quad (9a)$$

$$x_{l,t} \geq x_{l,t-1}. \quad (9b)$$

C. Subproblem 1 (SP1): Making the Solution Feasible

SP1 is designed to polish the investment solution obtained from the MP to make it feasible. At early iterations of the BD, to minimize (9a), all binary variables are usually set to zero (implying no candidate line is planned). When this investment plan is applied to SPs, power system constraints may be infeasible over the planning horizon because new lines may be needed to meet the load growth. Therefore, SP1, as formulated by (10) as a QC problem, is solved subject to power system constraints to remove infeasibilities. From physical point of view, it is possible to meet load growth by adding new lines as many as needed. Consequently, the internal loop of Fig. 1 converges after a few iterations when new lines are added to the network. In (10), $i, j \in \mathcal{V}_k$, $g \in \mathfrak{G}_k$, $l \in \mathcal{E}_k$, and $l \in \mathcal{L}_1$. In other words, (10) is satisfied for all islands $k \in \mathcal{K}$ (including the integrated system with $k = 1$).

$$\text{Min } f_{SP1} \geq \sum_{\forall k,i,t} (S1_{k,i,t} + S2_{k,i,t} + S3_{k,i,t} + S4_{k,i,t}). \quad (10a)$$

$$x_{l,t} = \overline{x_{l,t}} \rightarrow \lambda_{l,t}^{SP1}. \quad (10b)$$

$$\begin{aligned} & \sum_{\forall g} P_{k,g,t}^G a_{k,g,i,t} - \sum_{\forall l,j} P_{k,l,t} (b_{k,l,i,j} - b_{k,l,j,i}) \\ & = (1 - \psi_{k,i,t}) P_{i,t}^D + G_i^s \alpha_{k,i,t} + S1_{k,i,t} - S2_{k,i,t}. \end{aligned} \quad (10c)$$

$$\begin{aligned} & \sum_{\forall g} Q_{k,g,t}^G a_{k,g,i,t} - \sum_{\forall l,j} Q_{k,l,t} (b_{k,l,i,j} - b_{k,l,j,i}) \\ & = (1 - \psi_{k,i,t}) Q_{i,t}^D - B_i^s \alpha_{k,i,t} + S3_{k,i,t} - S4_{k,i,t}. \end{aligned} \quad (10d)$$

$$0 \leq \psi_{k,i,t} \leq 1. \quad (10e)$$

$$\begin{aligned} f_{k,\ell,t} & = G_\ell \sum_{\forall i} \alpha_{k,i,t} c_{k,\ell,i} - G_\ell \sum_{\forall i,j} \beta_{k,i,j,t} b_{k,\ell,i,j} \\ & \quad - B_\ell \sum_{\forall i,j} \gamma_{k,i,j,t} b_{k,\ell,i,j}. \end{aligned} \quad (10f)$$

$$\begin{aligned} g_{k,\ell,t} & = -B_\ell \sum_{\forall i} \alpha_{k,i,t} c_{k,\ell,i} + B_\ell \sum_{\forall i,j} \beta_{k,i,j,t} b_{k,\ell,i,j} \\ & \quad - G_\ell \sum_{\forall i,j} \gamma_{k,i,j,t} b_{k,\ell,i,j}. \end{aligned} \quad (10g)$$

$$f_{k,\ell,t} - M(1 - x_{\ell,t}) \leq P_{k,\ell,t} \leq f_{k,\ell,t} + M(1 - x_{\ell,t}). \quad (10h)$$

$$g_{k,\ell,t} - M(1 - x_{\ell,t}) \leq Q_{k,\ell,t} \leq g_{k,\ell,t} + M(1 - x_{\ell,t}). \quad (10i)$$

$$P_{k,\ell,t}^2 + Q_{k,\ell,t}^2 \leq x_{\ell,t} (S_\ell^U)^2. \quad (10j)$$

$$P_g^{GL} \leq P_{k,g,t}^G \leq P_g^{GU}. \quad (10k)$$

$$Q_g^{GL} \leq Q_{k,g,t}^G \leq Q_g^{GU}. \quad (10l)$$

$$(V_i^L)^2 \leq \alpha_{k,i,t} \leq (V_i^U)^2. \quad (10m)$$

$$\beta_{k,i,j,t} \tan \theta_{i,j}^L \leq \gamma_{k,i,j,t} \leq \beta_{k,i,j,t} \tan \theta_{i,j}^U. \quad (10n)$$

$$\beta_{k,i,j,t} = \beta_{k,j,i,t}. \quad (10o)$$

$$\gamma_{k,i,j,t} = -\gamma_{k,j,i,t}. \quad (10p)$$

$$\beta_{k,i,j,t}^2 + \gamma_{k,i,j,t}^2 \leq \alpha_{k,i,t} \alpha_{k,j,t}. \quad (10q)$$

Eq. (10a) minimizes the sum of non-negative slack variables $S1_{k,i,t}$, $S2_{k,i,t}$, $S3_{k,i,t}$, and $S4_{k,i,t}$ as power imbalance penalties that appear in (10c)–(10d). We assume that a generation expansion plan is already available and generators are added through $a_{k,g,i,t}$ over the planning period [25], [26]. A zero objective function f_{SP1} in (10a) implies that all power imbalances are mitigated. As shown in Fig. 1, the internal loop is iterated until f_{SP1} becomes zero. In (10b), binary decision variables $x_{l,t}$ are fixed to their optimal values $\overline{x_{l,t}}$ obtained by the MP in (9) in the previous iteration. This way, SP1 saves the QC feature by relaxing binary variables. In (10b), $\lambda_{l,t}^{SP1}$ indicates the associated dual variable, which will be used later in constructing Benders infeasibility cuts. These dual variables are the sensitivity of the objective function f_{SP1} with respect to variable $x_{l,t}$,

i.e. $\partial f_{SP1} / \partial x_{l,t}$ evaluated at $x_{l,t} = \overline{x_{l,t}}$. Dual values are usually accessible after solving the optimization problem using available solvers [27].

Power balance for each bus at every subgraph is established by (10c) and (10d), where the first term gives the total active/reactive generation at bus i and the second term is the total active/reactive power leaving bus i through existing and candidate lines. Active and reactive load shedding is also modeled in (10c) and (10d) by $\psi_{k,i,t}$ to keep islands stable after ICI. Load shedding limits are constrained by (10e). Slack variables in (10c) and (10d) model the generation deficiency and surplus. For instance, if $S1_{k,i,t}$ ($S2_{k,i,t}$) is nonzero in (10c), we have active generation surplus (deficiency) at bus i . Only one of $S1_{k,i,t}$ and $S2_{k,i,t}$ can be nonzero for a given bus i at period t in subgraph k (and similarly for $S3_{k,i,t}$ and $S4_{k,i,t}$). Equations (10f) and (10g) calculate auxiliary variables for active and reactive line flows, respectively. Equations (10h) and (10i) model active and reactive flows of lines using the big- M linearization technique to prevent bilinear terms (multiplication of binary and continuous variables). For existing lines, we have $x_{\ell,t} = 1$ in all planning periods.

To make the model convex, (10f) and (10g) employ variables $\alpha_{k,i,t}$, $\beta_{k,i,j,t}$, and $\gamma_{k,i,j,t}$ instead of commonplace variables of bus voltages and phase angles ($V_{k,i,t}$, $\theta_{k,i,t}$). The exact expressions for these transformed variables are $\alpha_{k,i,t} = V_{k,i,t}^2$, $\beta_{k,i,j,t} = V_{k,i,t} V_{k,j,t} \cos \theta_{k,i,j,t}$, and $\gamma_{k,i,j,t} = V_{k,i,t} V_{k,j,t} \sin \theta_{k,i,j,t}$, where $\theta_{k,i,j,t} = \theta_{k,i,t} - \theta_{k,j,t}$ [16]. If these exact nonlinear expressions had been incorporated into (10), SP1 would have been nonconvex. Alternatively, their relaxed forms are embedded in (10) to obtain a QC model of the network AC representation [15], [16].

The apparent ratings of lines are limited in (10j) as quadratic constraints. If a candidate line is not chosen (i.e., $x_{\ell,t} = 0$), (10j) enforces $P_{k,\ell,t} = Q_{k,\ell,t} = 0$. Thus, the flows of non-constructed candidate lines do not affect (10c) and (10d). Active and reactive power limits of generators are given in (10k) and (10l). Constraint (10m) bounds $\alpha_{k,i,t}$ within its limits. Constraint (10n) relates two relaxed variables $\beta_{k,i,j,t}$ and $\gamma_{k,i,j,t}$. Symmetric and skew-symmetric properties of $\beta_{k,i,j,t}$ and $\gamma_{k,i,j,t}$ are forced by (10o) and (10p), respectively. To strengthen the QC relaxation, the SOC requirement is imposed by (10q) [28]. Note that (10q) is convex in spite of having a bilinear term [16].

D. Subproblem 2 (SP2): Obtaining Optimal Operation Cost

After mitigating power imbalances by SP1, the operation cost is minimized in SP2. To do this, power generation costs of the integrated system (\mathcal{G}_1) and load shedding costs of islands ($\mathcal{G}_k, \forall k > 1$) are minimized as the first and second summations in (11a). Load shedding may be required to stabilize islands after ICI. The constraints of SP2, which is a QC problem, are given in (11b)–(11e).

$$\text{Min } f_{SP2} \geq \sum_{k=1,g,t} \frac{(P_{k,g,t}^G S_b) \tau_{k,t} C_g^{OP}}{(1+\sigma)^{t-1}} + \sum_{\forall k>1,i,t} \frac{(\psi_{k,i,t} P_{i,t}^D S_b) \tau_{k,t} \pi_t}{(1+\sigma)^{t-1}}. \quad (11a)$$

$$x_{l,t} = \overline{x_{l,t}} \rightarrow \lambda_{l,t}^{SP2}. \quad (11b)$$

$$\sum_{\forall g} P_{k,g,t}^G a_{k,g,i,t} - \sum_{\forall \ell,j} P_{k,\ell,t} (b_{k,\ell,i,j} - b_{k,\ell,j,i}) = (1 - \psi_{k,i,t}) P_{i,t}^D + G_i^s \alpha_{k,i,t}. \quad (11c)$$

$$\sum_{\forall g} Q_{k,g,t}^G a_{k,g,i,t} - \sum_{\forall \ell,j} Q_{k,\ell,t} (b_{k,\ell,i,j} - b_{k,\ell,j,i}) = (1 - \psi_{k,i,t}) Q_{i,t}^D - B_i^s \alpha_{k,i,t}. \quad (11d)$$

$$(10e)-(10q). \quad (11e)$$

Binary values obtained by the MP are fixed in (11b). Equations (11c) and (11d) are similar to (10c) and (10d), from which slack variables are removed. Considering Fig. 1, SP2 can be feasible without the slack variables since infeasibilities are already mitigated by SP1. Equations in (11e) model the remaining power system, TEP, and relaxation constraints similar to (10).

E. Subproblem 3 (SP3): Improving the Stability of Islands

The frequency deviations of generators from their island's COI frequency have been already obtained in (8). To establish more stable islands after ICI, total frequency deviations of generators at every island are minimized by SP3 as given in (12).

$$\text{Min } f_{SP3} \geq \sum_{\forall k>1,g,t} (S5_{k,g,t} + S6_{k,g,t}). \quad (12a)$$

$$x_{l,t} = \overline{x_{l,t}} \rightarrow \lambda_{l,t}^{SP3}. \quad (12b)$$

$$\Delta P_{k,g,t} = P_{k,g,t}^G - P_{g,t}^{G0}. \quad (12c)$$

$$\Delta \omega_{k,g,t} = \frac{\mu_g \Delta P_{k,g,t} \sum_{\forall g} H_g - \sum_{\forall g} (\mu_g H_g \Delta P_{k,g,t})}{\sum_{\forall g} H_g}. \quad (12d)$$

$$\Delta \omega_{k,g,t} + S5_{k,g,t} - S6_{k,g,t} = 0. \quad (12e)$$

$$(11c)-(11e). \quad (12f)$$

The objective function f_{SP3} in (12a) minimizes the sum of non-negative slack variables modeling frequency deviations of generators. Investment binary decisions are fixed in (12b) with the dual value $\lambda_{l,t}^{SP3}$. In (12c), $P_{g,t}^{G0}$ represents the active output power of generator g at period t before ICI (pre-islanding state) and $\Delta P_{k,g,t}$ is the change in the generator active power after islanding. The frequency deviations of generators after ICI are given by (12d). Positive slack variables in (12e) model the lag or lead of the frequency of generator g with respect to the COI frequency of the island. Only one of variables $S5_{k,g,t}$ and $S6_{k,g,t}$ can be nonzero for a given generator at a period in an island. By minimizing the sum of these slack variables in (12a), frequency deviations of generators after ICI are minimized. Although the objective function in (12a) may not ultimately be

zero, it will be minimized to improve the stability of the islands. Other constraints related to system operation, TEP, and relaxations are imposed by (12f).

F. Feasibility and Infeasibility Cuts

The MP objective including the SP2 feasibility cut is given in (13a). The SP2 feasibility cut is specified in (13b). Infeasibility cuts resulting from SP1 and SP3 are expressed by (13c) and (13d), respectively. These cuts are added to the MP in each iteration.

$$f_{MP} \geq \sum_{\forall l,t} \frac{IC_l(x_{l,t} - x_{l,t-1})}{(1+\gamma)^{t-1}} + \eta. \quad (13a)$$

$$\eta \geq \overline{f_{SP2}} + \sum_{\forall l,t} \lambda_{l,t}^{SP2} (x_{l,t} - \overline{x_{l,t}}). \quad (13b)$$

$$\overline{f_{SP1}} + \sum_{\forall l,t} \lambda_{l,t}^{SP1} (x_{l,t} - \overline{x_{l,t}}) \leq 0. \quad (13c)$$

$$\overline{f_{SP3}} + \sum_{\forall l,t} \lambda_{l,t}^{SP3} (x_{l,t} - \overline{x_{l,t}}) \leq 0. \quad (13d)$$

where $\overline{f_{SP1}}$, $\overline{f_{SP2}}$, and $\overline{f_{SP3}}$ parameters are the values obtained for objective functions SP1, SP2, and SP3, respectively. The feasibility cut η in (13a) steers the MP solution as the BD lower bound toward the BD upper bound to converge (as shown in Fig. 1). By adding cuts (13) at each iteration, SPs affect the MP optimal investment plan through their dual variables and objective functions.

Using the proposed solution scheme, the ICI-TEP problem is decomposed into smaller problems: the MP, SP1, SP2, and SP3 described by (9), (10), (11), and (12), respectively. The MP is a small ILP problem. Also, since binary variables $x_{l,t}$ are fixed to $\overline{x_{l,t}}$ in SPs, SPs are relaxed from binary variables and they represent QC problems. The MP and SPs can be efficiently solved using available solvers to achieve their global optimal solution within a proper optimality gap. However, the original ICI-TEP problem (without decomposition) represents a mixed-integer QC programming (MIQCP) problem that might be intractable. The integrated MIQCP model can be described as a multi-objective optimization problem:

$$\min(f_{MP} + f_{SP2}, f_{SP3}) \quad (14a)$$

$$\text{s.t. (9), (10e)-(10q), (11a), (11c)-(11d), (12a),$$

$$(12c)-(12e). \quad (14b)$$

IV. CASE STUDIES AND NUMERICAL RESULTS

To evaluate the performance of the proposed ICI-TEP method, its results are compared with those of the conventional TEP (C-TEP) method, in which ICI is separately performed. All optimization codes are implemented in GAMS 27.1.0 and solved by the GUROBI 8.1.1 solver on a personal computer with a 3.2 GHz i7 CPU and 16 GB of RAM. The maximum number of iterations in the inner and outer loops of Fig. 1 is set to 200. The case studies are examined with the BD convergence tolerance of 0% and 0.5%. Since the BD convergence tolerance is normalized by UB , it is possible to set its percentage value in

advance regardless of the system size. The cost of load shedding is assumed \$10,000/MWh [29]. For the generation expansion, we follow the basic generation expansion model of [19] to expand the capacity of existing power plants as an input to our proposed method.

A. IEEE 39-Bus Test System

A 5-year planning horizon with a 7% annual load growth is assumed for TEP on the modified IEEE 39-bus test system with a 20% increased loading level [19]. We have run the basic GEP model of [19] to expand the capacity of existing power plants using 197 MW generation units to meet the demand levels. As a result, for the IEEE 39-bus test system, we have obtained 12, 4, 5, 0, and 7 generation units to be installed in planning years 1, 2, 3, 4, and 5, respectively. This test system is shown in Fig. 2. Candidate branches (lines and transformers) are considered in existing corridors with the same specifications as existing branches. Time domain simulations are carried out by DIGSILENT software package. Types of AVR and governor are assumed as IEEE T1 and BPA GG, respectively [30]. We consider an islanding scenario in the third year initiated by a three-phase fault at line 2-3 near bus 2. This fault occurs at $t = 1$ sec and is cleared at $t = 1.65$ sec [1]. This fault-on period is probable if the primary protection relay fails to operate. After clearing the fault, three groups of coherent generators are formed [1]: {G31, G32}, {G33, G34, G35, G36}, and {G30, G37, G38, G39}, in which G_n denotes generator at bus n . If the system is not islanded following this fault, it experiences unacceptable operating conditions as depicted in Fig. 3. As seen from Fig. 3(a), after clearing the fault, G30, G37, G38, and G39 fail to reach stable angles. This situation mainly challenges the synchronism and thus threatens the angle and frequency stabilities of a power system. The instability of these four generators can also be seen from their rotor speeds in Fig. 3(b). Moreover, in Fig. 3(c), voltage magnitudes of some buses that experience larger voltage fluctuations are plotted for the period following the fault at $t = 1$ sec. Before occurring the fault, all voltages were in their permitted range [0.95, 1.05] pu. Shortly following the fault, voltages at some buses become as low as 0.2 pu, while after a few seconds, some buses such as 25, 26, and 27 experience voltage increase as high as 1.23 pu.

Note that although generator angles and speeds may be more important variables in islanding, voltage excursions should be also observed [10]. Consequently, if the network is not split into islands, global blackout may happen as a result of cascading trips caused by out-of-range generator angles and speeds as well as out-of-range voltages. However, using ICI, the network is split into three islands considering coherent generator groups as illustrated in Fig. 2 [1]. Therefore, in this ICI scenario, we have the main graph $k = 1$ corresponding to the pre-islanding system that includes all buses and subgraphs $k = 2, 3, 4$ corresponding to the three islands. To evaluate the accuracy of approximating (2) with (3), we have checked these equations for 10 generators in the IEEE 39-bus test system. The largest error is 2.1% happening at G39 that experiences the most varying term under the integration in (2). Other generators have lower approximation errors.

Planning results obtained by C-TEP and proposed ICI-TEP methods are presented in Table I. It is seen that the C-TEP

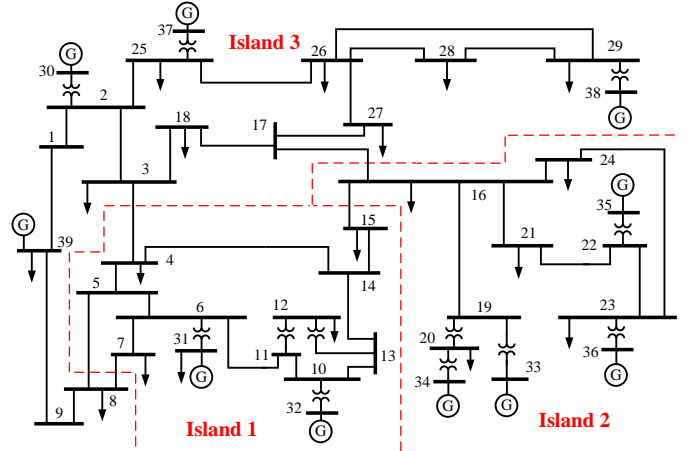


Fig. 2. One-line diagram of the IEEE 39-bus test system with its islands.

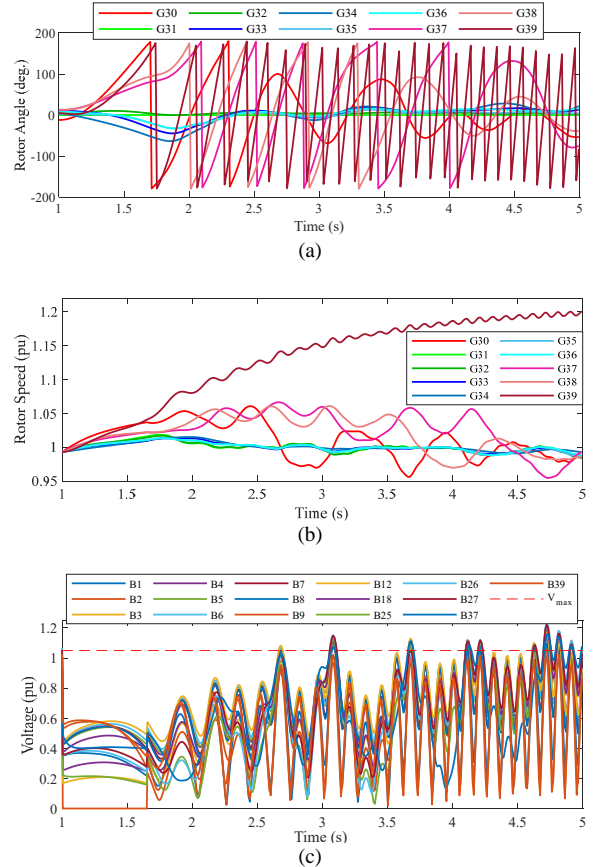


Fig. 3. Post-fault variables in the IEEE 39-bus system without islanding, (a) rotor angles, (b) rotor speeds, (c) critical voltages.

method has 7 planned lines with a total investment cost of \$15.5M. The total cost (including investment, load shedding, generation, and blackout costs) is \$6881.1M. After islanding, \$171.1M load shedding cost is yielded in C-TEP. The C-TEP method does not consider islanding scenarios while it plans lines. Thus, line 16–17, which is planned in the 2nd year, is a cut-set that is opened in the ICI (see Fig. 2). This implies that islands 2 and 3 may become more vulnerable after islanding due to opening of line 16–17.

On the other hand, the proposed ICI-TEP method plans 10 lines (1 line in the 2nd year, 7 lines in the 3rd year, and 2 lines in the 4th year) with the investment cost of \$33.1M. These lines

are planned to meet load growth and to reinforce the network against the ICI. Although this investment cost is higher than that of the C-TEP method, a lower load shedding cost of \$131.2M is needed (23.3% lower than C-TEP). The three additional lines make it possible to reduce the load shedding. Using the investment cost of 197MW units [19], the generation expansion cost for this test system is obtained as \$2,255.96M, which is about 36% of the ICI-TEP total cost.

It is worthwhile to note that both methods of C-TEP and ICI-TEP have used load shedding to maintain load-generation balance in islands. However, the transient behavior and the stability of the solutions in Table I should also be analyzed by time-domain simulations.

Time-domain simulation results of the ICI-TEP solution are shown in Fig. 4. To easily discriminate generators of islands in Fig. 4, the curves of the generators in islands 1, 2, and 3 are depicted with green, blue, and red based colors. The largest angular oscillation in Fig. 4(a) occurs in the generators of island 3 {G30, G37, G38, G39}. As seen in Fig. 4(b), islands 1, 2, and 3 finally approach their own steady-state frequencies as 1.000637, 1.00361, and 0.988458 pu, respectively. All islands are stable although island 3 experiences a more difficult situation with larger angular fluctuations and a lower steady-state frequency. In addition, all voltages in the three islands are in their normal range [0.95,1.05] pu; therefore, there is no voltage security problem such as tripping of devices due to out of range voltages. Consequently, the proposed ICI-TEP method has been able to save the stability of islands by appropriately reinforcing the transmission system as the backbone of islands. Thus, it has zero blackout cost as specified in Table I.

Time-domain simulation results of the C-TEP solution are depicted in Fig. 5. Islands 1 and 2 can converge to a new stable point with their own steady-state frequencies as 1.000663 and 1.000344 pu, respectively. However, as seen in Fig. 5(a), all four generators of island 3 {G30, G37, G38, G39} have rotor angle fluctuations making island 3 unstable. Considering Fig. 5(b), G39 (which is the largest generator of the system) accelerates its speed and has to be finally separated from other generators of the island. These four generators in island 3 fail to converge to a common speed and thus, frequency of island 3 becomes unstable. One reason is that the transmission system of this island is not strong enough at the ICI time. Although line 16–17 is planned by the C-TEP method (Table I), it is opened in the ICI and therefore island 3 becomes vulnerable. Comparison of Fig. 4 and Fig. 5 validates the resiliency and stability improvement of the ICI-TEP solution.

As a result of blackout in island 3, its total load has to be shed resulting in the blackout cost $C_B = \$566.9M$ (Table I), which is much higher than the investment cost of C-TEP (\$15.5M). This blackout cost, caused by the instability of island 3, incurs an unintentional significant load shedding cost, which is different from the intentional load shedding cost C_{LS} that is used to maintain load-generation balance in islands. This shows that although the C-TEP method has lower investment cost compared with the proposed ICI-TEP method, it results in significant financial losses as it fails to establish stable islands encountering major disturbances. As reported in Table I, the proposed ICI-TEP method results in the total cost of \$6293.4M,

TABLE I
PLANNING AND OPERATION RESULTS OF THE IEEE 39-BUS TEST CASE

Method	Planned Lines	$C_I, C_G, C_{LS}, C_B, C_T$ (M\$)
C-TEP	Y2: 16–17. Y4: 7–8, 14–15. Y5: 4–14, 10–13, 10–32, 13–14.	15.5, 6127.6, 171.1, 566.9, 6881.1
Proposed ICI-TEP	Y2: 3–18. Y3: 9–39, 10–13, 13–14, 14–15, 17–27, 25–26, 26–27. Y4: 4–14, 10–32.	33.1, 6129.1, 131.2, 0, 6293.4

Y_n : planning year n . C_I : Investment cost. C_G : Generation cost. C_{LS} : Load shedding cost. C_B : Blackout cost. C_T : Total cost.

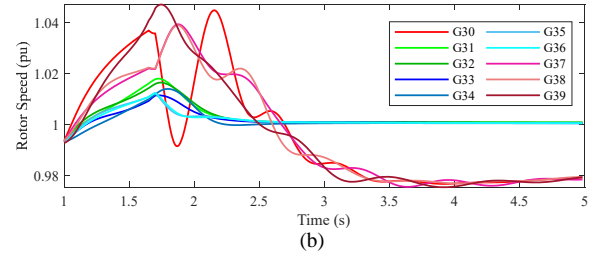
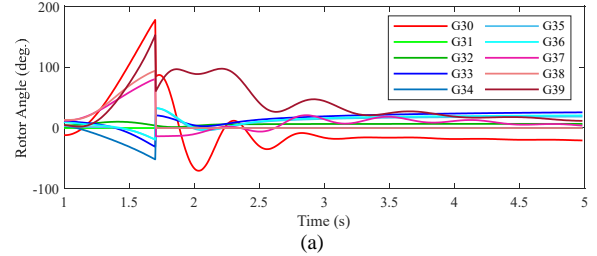


Fig. 4. Time domain simulation results of ICI-TEP solution, (a) rotor angles, (b) generator speeds.

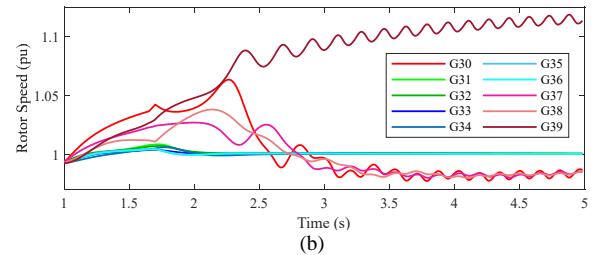
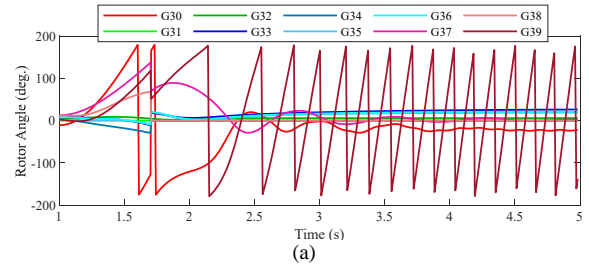


Fig. 5. Time domain simulation results of C-TEP solution, (a) rotor angles, (b) generator speeds.

which is 8.5% lower than that of the C-TEP method (\$6881.1M).

The computation times, as reported by GAMS, are 56.4 and 63.2 sec for the C-TEP and ICI-TEP methods, respectively, with a zero BD convergence tolerance. Since the ICI-TEP solves the integrated network and islands simultaneously, its computation burden is slightly higher than C-TEP. The computation time of the integrated MIQCP model (14) is 1123 sec (18.7 min) for this test case.

B. IEEE 300-Bus Test System

This test system, which has 300 buses, 411 branches, and 69 generators, is chosen to evaluate the scalability of the proposed method. The criteria that are considered for candidate lines, load growth, and planning years are similar to those already explained in Subsection IV-A. The generation expansion plan is assumed to install 197 MW units with the numbers of 6, 10, and 10 at planning years 3, 4, and 5, respectively. Two ICI scenarios are assumed to occur in the 2nd and 4th years as shown in Table II [7].

The results of C-TEP and ICI-TEP are presented in Table III. To save space, only the number of planned lines in each year is provided. The total number of planned lines with the C-TEP and ICI-TEP methods is 50 and 56, respectively. Investment costs obtained by the C-TEP and proposed ICI-TEP methods are \$616.8M and \$623.0M, respectively. Although the cost and number of planned lines of ICI-TEP method are slightly higher than those of C-TEP method, it leads to a significantly lower load shedding cost (\$5.0M versus \$64.4M) due to providing more reinforced islands. As seen in Table III, the proposed ICI-TEP method has 37/51 new lines available in the ICI of the 2nd/4th year versus 33/45 new lines available in C-TEP method. Because the additional new lines of the ICI-TEP method are planned considering the ICI scenarios, the load shedding cost is significantly decreased by more than 92.2% compared with C-TEP method. Using the investment cost of 197MW units [19], the generation expansion cost for this test system is obtained as \$2,094.82M, which is about 13% of the ICI-TEP total cost in Table III.

The computation times for the ICI-TEP and C-TEP methods are 2195.7 and 1389.2 sec, respectively, with a 0.5% BD convergence tolerance. Considering a zero BD convergence tolerance, the computation times become 3403.4 and 2125.3 sec for the ICI-TEP and C-TEP, respectively. These execution times are competing for a planning problem implying the scalability of the models. However, the integrated MIQCP model (14) could not be solved even after 24 hours execution time implying the effectiveness of the proposed BD strategy to make the problem tractable.

V. CONCLUSIONS

In this paper, the performance of TEP is enhanced by incorporating ICI scenarios to increase the resiliency of power systems in case of major disturbances resulting in islanding. A criterion based on the COI frequency of islands is also proposed to improve the frequency stability of islands after splitting the network. The proposed ICI-TEP method is formulated as a convex model using AC network representation. The numerical experiments illustrate that: 1) compared to conventional TEP method, the proposed ICI-TEP method, by a slightly higher investment cost, not only reduces the intentional load shedding cost, but also avoids unintentional significant load shedding cost (blackout cost) because of planning a more reinforced transmission network leading to more stable islands encountering major disturbances, and 2) The proposed ICI-TEP method has high scalability as its computation time for the IEEE 300-bus test system with a 5-year planning horizon is only 36.6 minutes.

TABLE II
ICI SCENARIOS FOR THE IEEE 300-BUS TEST SYSTEM

ICI Period	Cut-sets
Year 2	{109–110, 122–123, 109–129}
Year 4	{109–110, 122–123, 109–129}, {57–66, 64–67, 66–190, 68–173, 174–191, 174–198, 184–185, 185–187}

TABLE III
PLANNING AND OPERATION RESULTS OF IEEE 300-BUS TEST SYSTEM

Method	Number of Planned Lines	C_I, C_{LS}, C_T (M\$)
C-TEP	Y1: 21, Y2: 12, Y3: 8, Y4: 4, Y5: 5.	616.8, 64.4, 16670.3
ICI-TEP	Y1: 22, Y2: 15, Y3: 7, Y4: 7, Y5: 5.	623.0, 5.0, 16625.9

Y_n: planning year *n*. C_I : Investment cost. C_{LS} : Load shedding cost. C_T : Total cost.

REFERENCES

- [1] P. Demetriou, M. Asprou, and E. Kyriakides, "A real-time controlled islanding and restoration scheme based on estimated states," *IEEE Trans. Power Syst.*, vol. 34, no. 1, pp. 606–615, 2019, doi: 10.1109/TPWRS.2018.2866900.
- [2] P. Kundur and C. W. Taylor, "Blackout experiences and lessons, best practices for system dynamic performance, and the role of new technologies," *IEEE Task Force Rep.*, 2007.
- [3] USA Today, "Power restored after partial New York City blackout leaves thousands without electricity." www.usatoday.com (accessed Jul. 23, 2019).
- [4] IEEE Standard, *C37.113-2015: IEEE guide for protective relay applications to transmission lines*. 2015.
- [5] X. Li, L. Ding, G. Zhu, and M. Kheshti, "Transient instability detection method based on multi-source trajectory information," *Int. J. Electr. Power Energy Syst.*, vol. 113, pp. 897–905, 2019, doi: 10.1016/j.ijepes.2019.06.009.
- [6] G. Patsakis, D. Rajan, I. A. Aravena Solis, and S. Oren, "Strong mixed-integer formulations for power system islanding and restoration," *IEEE Trans. Power Syst.*, vol. 34, no. 6, pp. 4880–4888, 2019, doi: 10.1109/TPWRS.2019.2920872.
- [7] A. Kyriacou, P. Demetriou, C. Panayiotou, and E. Kyriakides, "Controlled islanding solution for large-scale power systems," *IEEE Trans. Power Syst.*, vol. 33, no. 2, pp. 1591–1602, 2018, doi: 10.1109/TPWRS.2017.2738326.
- [8] M. Ghamsari-Yazdel, M. Esmaili, F. Aminifar, P. Gupta, A. Pal, and H. Shayanfar, "Incorporation of controlled islanding scenarios and complex substations in optimal WAMS design," *IEEE Trans. Power Syst.*, vol. 34, no. 5, pp. 3408–3416, 2019, doi: 10.1109/TPWRS.2019.2901748.
- [9] P. A. Trodden, W. A. Bukhsh, A. Grothey, and K. I. M. McKinnon, "Optimization-based islanding of power networks using piecewise linear AC power flow," *IEEE Trans. Power Syst.*, vol. 29, no. 3, pp. 1212–1220, 2014, doi: 10.1109/TPWRS.2013.2291660.
- [10] P. Kundur *et al.*, "Definition and classification of power system stability," *IEEE Trans. Power Syst.*, vol. 19, no. 3, pp. 1387–1401, 2004, doi: 10.1109/TPWRS.2004.825981.
- [11] J. Zhao, Y. Tang, and V. Terzija, "Robust online estimation of power system center of inertia frequency," *IEEE Trans. Power Syst.*, vol. 34, no. 1, pp. 821–825, 2019, doi: 10.1109/TPWRS.2018.2879782.
- [12] F. Milano, "Rotor speed-free estimation of the frequency of the center of inertia," *IEEE Trans. Power Syst.*, vol. 33, no. 1, pp. 1153–1155, 2018, doi: 10.1109/TPWRS.2017.2750423.
- [13] H. Golpîra and A. R. Messina, "A center-of-gravity-based approach to estimate slow power and frequency variations," *IEEE Trans. Power Syst.*, vol. 33, no. 1, pp. 1026–1035, 2018, doi: 10.1109/TPWRS.2017.2710187.
- [14] P. A. Trodden, W. A. Bukhsh, A. Grothey, and K. I. M. McKinnon, "MILP formulation for controlled islanding of power networks," *Int. J. Electr. Power Energy Syst.*, vol. 45, no. 1, pp. 501–508, 2013, doi: 10.1016/j.ijepes.2012.09.018.
- [15] C. Coffrin, R. Bent, B. Tasseff, K. Sundar, and S. Backhaus, "Relaxations of AC maximal load delivery for severe contingency analysis," *IEEE Trans. Power Syst.*, vol. 34, no. 2, pp. 1450–1458, 2019, doi: 10.1109/TPWRS.2018.2876507.
- [16] M. Bynum, A. Castillo, J. P. Watson, and C. D. Laird, "Tightening McCormick relaxations toward global solution of the ACOFP problem," *IEEE Trans. Power Syst.*, vol. 34, no. 1, pp. 814–817, 2019, doi: 10.1109/TPWRS.2018.2877099.

- [17] S. Dehghan, N. Amjady, and A. J. Conejo, "A multistage robust transmission expansion planning model based on mixed binary linear decision rules - Part I," *IEEE Trans. Power Syst.*, vol. 33, no. 5, pp. 5341–5350, 2018, doi: 10.1109/TPWRS.2018.2799946.
- [18] H. Haghighat and B. Zeng, "Bilevel conic transmission expansion planning," *IEEE Trans. Power Syst.*, vol. 33, no. 4, pp. 4640–4642, 2018, doi: 10.1109/TPWRS.2018.2835663.
- [19] M. Esmaili, M. Ghamsari-Yazdel, N. Amjady, and A. J. Conejo, "Short-circuit constrained power system expansion planning considering bundling and voltage levels of lines," *IEEE Trans. Power Syst.*, vol. 35, no. 1, pp. 584–593, 2020, doi: 10.1109/TPWRS.2019.2926410.
- [20] Y. Liu, R. Sioshansi, and A. J. Conejo, "Multistage stochastic investment planning with multiscale representation of uncertainties and decisions," *IEEE Trans. Power Syst.*, vol. 33, no. 1, pp. 781–791, 2018, doi: 10.1109/TPWRS.2017.2694612.
- [21] M. Ahmadigorji, N. Amjady, and S. Dehghan, "A robust model for multiyear distribution network reinforcement planning based on information-gap decision theory," *IEEE Trans. Power Syst.*, vol. 33, no. 2, pp. 1339–1351, 2018, doi: 10.1109/TPWRS.2017.2732447.
- [22] A. J. Wood, B. F. Wollenberg, and G. B. Sheble, *Power Generation, Operation, and Control*. Wiley, 2013.
- [23] K. R. Padiyar, *Power system dynamics: stability and control*, 2nd ed. Hyderabad, India: BS Publications, 2008.
- [24] H. You, V. Vittal, and X. Wang, "Slow coherency-based islanding," *IEEE Trans. Power Syst.*, vol. 19, no. 1, pp. 483–491, 2004, doi: 10.1109/TPWRS.2003.818729.
- [25] A. Lotfjou, Y. Fu, and M. Shahidehpour, "Hybrid AC/DC transmission expansion planning," *IEEE Trans. Power Deliv.*, vol. 27, no. 3, pp. 1620–1628, 2012, doi: 10.1109/TPWRD.2012.2194515.
- [26] P. V. Gomes and J. T. Saraiva, "State-of-the-art of transmission expansion planning: A survey from restructuring to renewable and distributed electricity markets," *Int. J. Electr. Power Energy Syst.*, vol. 111, pp. 411–424, 2019, doi: 10.1016/j.ijepes.2019.04.035.
- [27] R. E. E. Rosenthal, M. R. Bussieck, and A. Meeraus, *General algebraic modeling system (GAMS)*. Washington, DC, USA: GAMS Development Corporation, www.gams.com, 2019.
- [28] C. Coffrin, H. L. Hijazi, and P. Van Hentenryck, "Strengthening the SDP relaxation of AC power flows with convex envelopes, bound tightening, and valid inequalities," *IEEE Trans. Power Syst.*, vol. 32, no. 5, pp. 3549–3558, 2017, doi: 10.1109/TPWRS.2016.2634586.
- [29] O. Ziaee, O. Alizadeh-Mousavi, and F. F. Choobineh, "Co-optimization of transmission expansion planning and TCSC placement considering the correlation between wind and demand scenarios," *IEEE Trans. Power Syst.*, vol. 33, no. 1, pp. 206–215, 2018, doi: 10.1109/TPWRS.2017.2690969.
- [30] F. Teymouri, T. Amraee, H. Saberi, and F. Capitanescu, "Toward controlled islanding for enhancing power grid resilience considering frequency stability constraints," *IEEE Trans. Smart Grid*, vol. 10, no. 2, pp. 1735–1746, 2019, doi: 10.1109/TSG.2017.2777142.